

가

VX2  
Oxide

MRI

Superparamagnetic Iron  
Sequence<sup>1</sup>

2 . . . 3 . .

superparamagnetic iron oxide  
(SPIO) MRI  
VX2 MRI  
SPIO MRI  
(7 msec, 12 msec, 15 msec, 35 msec) T2\*  
4 가 ,  
T2 (35 msec) T2\* (12 msec)  
T2\* 가  
msec) T2\* 가  
(12 msec) (76%) 가  
(86% - 97%) 가  
SPIO MRI T2  
(12 msec) T2\* 가  
가 가

(6 - 8), SPIO MRI가  
가 CTAP (8 - 10) SPIO MRI가 가  
가 가  
(1). Superparamagnetic iron oxide (SPIO) (Kupffer cell) SPIO  
T2 (8, 11 - 13)  
가 가

(2 - 4), 가

가 (5).

arterial portography (CTAP)가 가 CT

(14 - 19).  
가

VX2  
SPIO

MRI

가

2002 3 6

2002 8 21





**Table 4.** Sensitivity of VX2 Carcinomas for SPIO-Enhanced MR Images with Various Pulse Sequences

Sequence	Number of True Positive Nodules Detected at MRI			Sensitivity (%)			Rank (Overall)
	Overall	< 5 mm	< 10 mm	Overall	< 5 mm	< 10 mm	
FLASH (TE 12, FA 30 <sub>o</sub> )	32	7	24	84	70	83	1
FISP (TE 12)	31	6	22	82	60	76	2
TSE T2	30	8	21	79	80	72	3
TSE PD	29	8	21	76	80	72	4
FLASH (TE 15, FA 30 <sub>o</sub> )	27	4	19	71	40	66	5
FLASH(TE 7, FA 30 <sub>o</sub> )	25	3	16	66	30	55	6
FISP (TE 7)	24	3	15	63	30	52	7
FLASH(TE 12, FA 80 <sub>o</sub> )	20	1	12	53	10	41	8
FLASH(TE 35, FA 30 <sub>o</sub> )	19	3	13	50	30	45	9

Note. The total number of VX2 carcinomas in the pathologic specimen was 38; those smaller than or equal to 10 mm were 29 and those smaller than or equal to 5 mm were 10. There were significant ( $p < .05$ ) differences of overall detection sensitivity in the following comparisons (numbers indicate rank): the sequences ranked 1 - 3 vs. 5 - 9 and the sequence ranked 4 vs. 6 - 9.

**Table 5.** Positive Predictive Value of VX2 Carcinomas for SPIO-Enhanced MR Images with Various Pulse Sequences

Sequence	Number True Positive Nodules	False Positive Nodules	Positive Predictive Value (%)
TSE T2	29	1	97
FLASH (TE 35, FA 30 <sub>o</sub> )	19	1	95
TSE PD	30	2	94
FLASH (TE 15, FA 30 <sub>o</sub> )	27	2	93
FISP (TE 12)	31	3	91
FISP (TE 7)	24	3	89
FLASH (TE 12, FA 30 <sub>o</sub> )	32	4	89
FLASH (TE 12, FA 80 <sub>o</sub> )	20	3	87
FLASH (TE 7, FA 30 <sub>o</sub> )	25	4	86

Note. There was no statistically significant difference between the values of each sequence ( $p > .05$ ).

T2\* 가 (Fig. 2).  
 가  
 10 mm  
 5 mm MR (partial volume averaging effect)  
 가

SPIO  
 80%가  
 6%가 (20).  
 가  
 T2 (2 - 4).  
 가 (5).  
 가 (size threshold)  
 가 (75 - 96%) (15, 21, 22).  
 50 - 84%  
 가

1 cm

3/4 가 (29/38)

가

SPIO

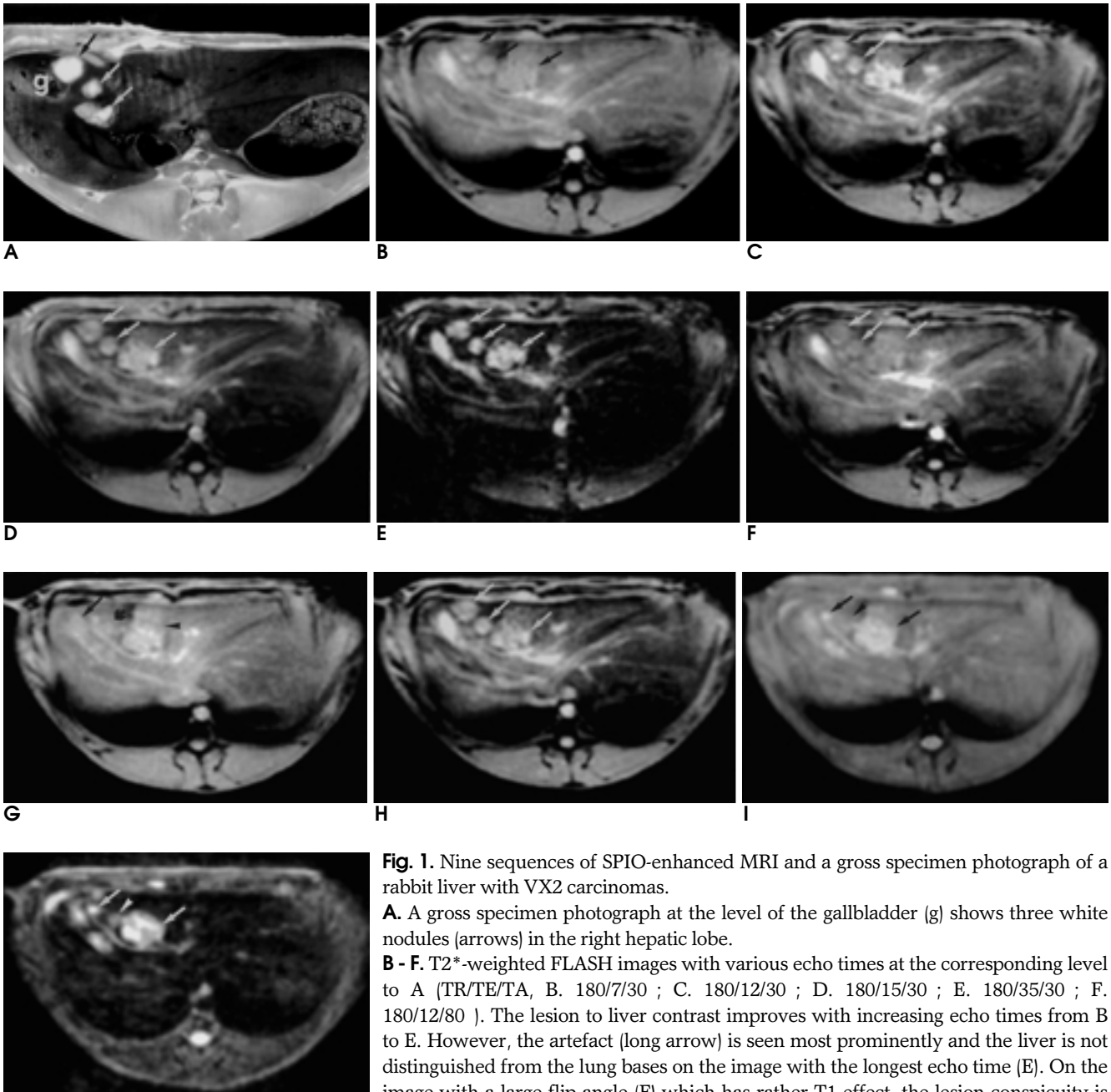


**Fig. 1.** Nine sequences of SPIO-enhanced MRI and a gross specimen photograph of a rabbit liver with VX2 carcinomas.

**A.** A gross specimen photograph at the level of the gallbladder (g) shows three white nodules (arrows) in the right hepatic lobe.

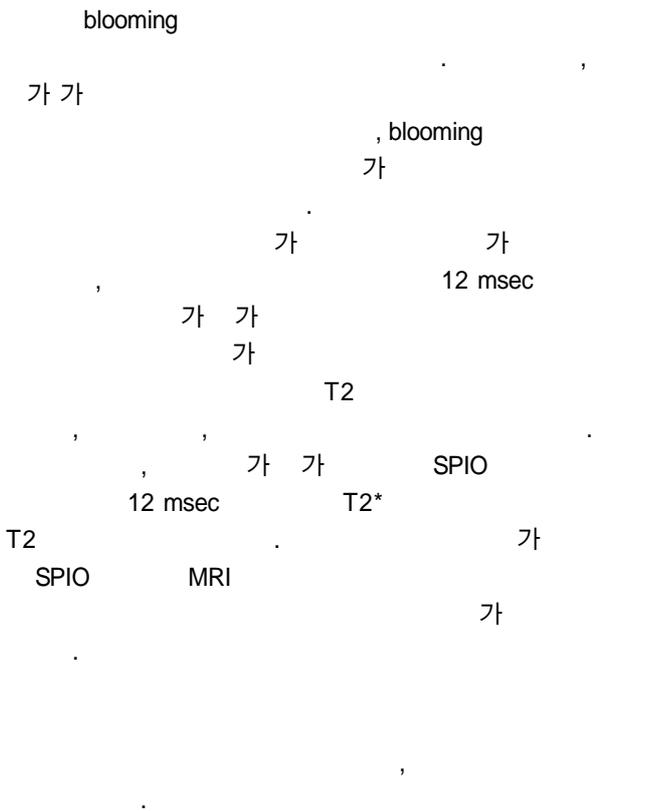
**B - F.** T2\*-weighted FLASH images with various echo times at the corresponding level to A (TR/TE/TA, B. 180/7/30°, C. 180/12/30°; D. 180/15/30°; E. 180/35/30°; F. 180/12/80°). The lesion to liver contrast improves with increasing echo times from B to E. However, the artefact (long arrow) is seen most prominently and the liver is not distinguished from the lung bases on the image with the longest echo time (E). On the image with a large flip angle (F) which has rather T1 effect, the lesion conspicuity is markedly inferior to that on C with the same echo time but a smaller flip angle.

**G.** On T2\*-weighted FISP image with short echo time (TR/TE/FA, 180/7/30°), one (short arrow) of three tumors was not detected during image analysis and the margin of the largest tumor (arrowhead) is markedly blurred.

**H.** T2\*-weighted FISP image with medium echo time (TR/TE/FA, 180/12/30°), shows better lesion conspicuity and image quality compared with G.

**I, J.** Proton density weighted (I: TR/TE/ETL, 4500/16/5) and T2-weighted (J: TR/TE/ETL, 4500/98/5) turbo spin echo sequences show excellent lesion conspicuity. One of the tumors (arrowhead) is poorly delineated on this slice but clearly seen on the next caudal image (not shown). T2-weighted image (J) provides the superior lesion contrast but shows rather prominent imaging artefact compared with other sequences (G - I). Also noted the blurred hepatic margin.





1. Brasch RC. New directions in the development of MR imaging contrast media. *Radiology* 1992;183:1-11
2. Saini S, Stark DD, Hahn PF, et al. Ferrite particles: a superparamagnetic MR contrast agent for enhanced detection of liver carcinoma. *Radiology* 1987;162:217-222
3. Petersein J, Saini S, Weissleder R. Liver II: Iron oxide-based reticuloendothelial contrast agents for MR imaging clinical review. *Magn Reson Imaging Clin N Am* 1996;4:53-60
4. Hahn PF, Saini S. Liver-specific MR imaging contrast agents. *Radiol Clin North Am* 1998;36:287-297
5. Stark DD, Weissleder R, Elizondo G, et al. Superparamagnetic iron oxide: clinical application as a contrast agent for MR imaging of the liver. *Radiology* 1988;168:297-301
6. Nelson RC, Chezmar JL, Sugarbaker PH, Bernardino ME. Hepatic tumors: comparison of CT during arterial portography, delayed CT, and MR imaging for preoperative evaluation. *Radiology* 1989;172:27-34
7. Heiken JP, Weyman PJ, Lee LKT, et al. Detection of focal hepatic masses: prospective evaluation with CT, delayed CT, CT during arterial portography, and MR imaging. *Radiology* 1989;171:47-51
8. Seneterre E, Taourel P, Bouveir Y, et al. Detection of hepatic metastases: ferumoxides-enhanced MR imaging versus unenhanced MR imaging and CT during arterial portography. *Radiology* 1996;200:785-792
9. : Gd-DTPA  
SPIO  
2000;42:265-272

10. Choi D, Kim SH, Lim JH, et al. Preoperative detection of hepatocellular carcinoma: ferumoxides-enhanced MR imaging versus combined helical CT during arterial portography and CT hepatic arteriography. *AJR Am J Roentgenol* 2001;176:475-482
11. Hagspiel KD, Neidl KF, Eichenberger AC, Weder W, Marinecek B. Detection of liver metastases: comparison of superparamagnetic iron oxide-enhanced and unenhanced MR imaging at 1.5 T with dynamic CT, intraoperative US, and percutaneous US. *Radiology* 1995;196:471-478
12. Ros PR, Freeny P, Harms SE, et al. Hepatic MR imaging with ferumoxides: a multicenter clinical trial of the safety and efficacy in the detection of focal hepatic lesions. *Radiology* 1995;196:481-488
13. Yamamoto H, Yamashita Y, Yoshimatsu S, et al. Hepatocellular carcinoma in cirrhotic livers: detection with unenhanced and iron oxide-enhanced MR imaging. *Radiology* 1995;195:106-112
14. Ward J, Chen F, Guthrie JA, et al. Hepatic lesion detection after superparamagnetic iron oxide enhancement: comparison of five T2-weighted sequences at 1.0T by using alternative-free response receiver operating characteristic analysis. *Radiology* 2000;214:159-166
15. SPIO MR : MR  
2000;42:787-796
16. Fretz CJ, Elizondo G, Weissleder R, Hahn PF, Stark DD, Ferrucci JT Jr. Superparamagnetic iron oxide-enhanced MR imaging: pulse sequence optimization for detection of liver cancer. *Radiology* 1989;172:393-397
17. Van Beers BE, Lacrosse M, Jamart J, et al. Detection and segmental location of malignant hepatic tumors: comparison of ferumoxides-enhanced gradient-echo and T2-weighted spin-echo MR imaging. *AJR Am J Roentgenol* 1997;168:713-717
18. Jung G, Krahe T, Kugel H, et al. Detection of focal hepatic lesions: effects of superparamagnetic iron oxide (AMI-25) on magnetic resonance imaging of the liver using T2-weighted fast spin-echo sequences and gradient- and spin-echo sequences at 1.0 Tesla. *Invest Radiol* 1998;33:61-67
19. Abe Y, Yamashita Y, Namimoto T, Tang Y, Takahashi M. The value of fast and ultrafast T2-weighted MR imaging sequences in hepatic enhancement with ferumoxides: comparison with conventional spin-echo sequence. *Radiat Med* 2000;18:97-105
20. Weissleder R, Hahn PF, Stark DD, et al. Superparamagnetic iron oxide: enhanced detection of splenic tumors with MR imaging. *Radiology* 1988;169: 399-403
21. Oudkerk M, Van den Heuvel AG, Wielopolski PA, Schitz PI, Borel Rinkes IH, Wiggers T. Hepatic lesions: detection with ferumoxides-enhanced T1- weighted MR imaging. *Radiology* 1997;203:447-456
22. Ward J, Naik KS, Guthrie JA, Wilson D, Robinson PJ. Hepatic lesion detection: comparison of MR imaging after the administration of superparamagnetic iron oxide with dual-phase CT by using alternative-free response receiver operating characteristic analysis. *Radiology* 1999;210:459-466
23. Schwartz LH, Seltzer SE, Tempany CM, et al. Superparamagnetic iron oxide hepatic MR imaging: efficacy and safety using conventional and fast spin echo pulse sequences. *J Magn Reson Imaging* 1995;5:566-570
24. Reimer P, Rummeny EJ, Daldrup HE, et al. Clinical results with Resovist: a phase 2 clinical trial. *Radiology* 1995;195:489-496

## Pulse Sequence Optimization for Superparamagnetic Iron Oxide-enhanced MR Imaging in the Detection of Hepatic VX2 Tumors in Rabbits<sup>1</sup>

Hyun-Jung Jang, M.D.<sup>2</sup>, Joon Koo Han, M.D., Kyoung Ho Lee, M.D., Tae Kyoung Kim, M.D.<sup>3</sup>,  
Se Hyung Kim, M.D., Byung Ihn Choi, M.D.

<sup>1</sup>Department of Radiology, Seoul National University College of Medicine and the Institute of Radiation Medicine,

<sup>2</sup>Radiation Medicine Branch and Center for Liver Cancer, National Cancer Center,

<sup>3</sup>Department of Diagnostic Radiology, Asan Medical Center, University of Ulsan College of Medicine

**Purpose:** The purpose of this experimental study was to determine the optimal pulse sequences for SPIO-enhanced MR imaging in the evaluation of multiple hepatic tumors.

**Materials and Methods:** Twelve rabbits with multiple VX2 liver tumors underwent SPIO-enhanced MRI using the following nine pulse sequences: TSE T2-weighted imaging (T2WI), TSE proton density-weighted imaging (PDWI), and GRE T2\*-weighted imaging (T2\*WI) with seven different echo times (TE). Liver-lesion contrast-to-noise ratios (CNRs) were calculated, and images were also assessed qualitatively by two radiologists, who reached a consensus as to lesion conspicuity and imaging artefacts using a four-level scale. By means of pathologic correlation, the sensitivity and positive predictive value of each sequence was calculated.

**Results:** TSE T2WI and long-TE (35 msec) FLASH T2\*WI showed the highest liver-lesion CNR. The best lesion conspicuity was seen at TSE T2WI and medium-TE (12 msec) GRE T2\*WI. Short TE GRE T2\*WI showed the least imaging artefacts. The four sequences which demonstrated the best sensitivity were medium-TE (12 msec), GRE T2\*WI (FLASH, 84%; FISP, 82%), TSE T2WI (79%), and TSE PDWI (76%). All nine sequences showed overall high positive predictive value (86 - 97%), with no statistically significant difference ( $p > 0.05$ ).

**Conclusion:** In terms of image quality and the detection of sensitivity, TSE T2WI and medium TE (12 msec) GRE T2\*WI were the top two pulse sequences among the various sequences used for on SPIO-enhanced MRI. They are thus considered to be the optimal sequences for evaluating multiple malignant hepatic tumors.

**Index words :** Liver, neoplasms

Magnetic resonance (MR), contrast media

Address reprint requests to : Joon Koo Han, M.D., Department of Radiology, Seoul National University Hospital  
28, Yongon-dong, Chongno-gu, Seoul 110-744, Korea.  
Tel. 82-2-760-2584 Fax. 82-2-743-6358 E-mail: hanjk@radcom.snu.ac.kr